A Ripple-Based Design-Oriented Approach for Predicting Fast-Scale Instability in DC-DC Switching Power Supplies

E. Rodriguez, *Student Member, IEEE,* A. El Aroudi, *Member, IEEE,* F. Guinjoan *Member, IEEE,* E. Alarcón, *Member, IEEE*

***Abstract*—This paper presents a design-oriented analytical approach for predicting fast-scale instability in power electronics converters under voltage-mode control strategy. This approach is based on the use of the ripple amplitude of the feedback control voltage as an index for predicting subharmonic oscillations in these systems. First, the work revisits the stability analysis technique based on the nonlinear discrete-time model, demonstrating that the ripple amplitude can be included within the expression of the Jacobian matrix of this model, hence giving a mathematical support to extend the ripple index to more complex topologies. A simple but representative buck converter under voltage-mode control is used to illustrate the approach. Using the ripple-based index, closed-form expressions of stability boundaries are derived. Unlike other available results obtained from existing methods, the stability boundary, in this work is expressed analytically in terms of both power stage and controller design parameters. Moreover, one can determine how these parameters are involved in the closed form expressions and, furthermore, how each parameter affects the stability of the system. The approach is validated by numerical simulations from the state equations and also experimentally within a wide range of the design parameter space.**

I. Introduction

Switching power converters are widely used in many applications due to their high efficiency, small size and low cost and weight [1]. However, one of their main drawbacks is their switching nonlinearity making them prone to exhibit a large variety of complex behaviors. Consider the buck converter depicted in Fig. 1(a). It is in principle desirable that the system operates periodically with a constant switching frequency equal to that of the external sawtooth ramp signal $h(t)$ (Fig. 1(b)). However, under parameter changes, the stability of this operating mode can be lost resulting in bifurcation phenomena leading to subharmonic oscillations [2], quasi-periodic regimes [3] and chaotic behavior [4], [5]. These phenomena have been considered as undesired instabilities in these systems and their prediction has interested researchers during the last two decades. The most known instabilities are period-doubling bifurcations and Neimark-Sacker which are shown in Fig. 1(c) and Fig. 1(d) respectively. The first one, so-called Fast-Scale Instability (FSI), yields to subharmonic oscillations that eventually can end up in a chaotic regime after a cascade of period doubling and border collision bifurcations [2], [4]. The second one, so-called Slow-Scale Instability (SSI), yields to oscillations of the system state variables with relatively large

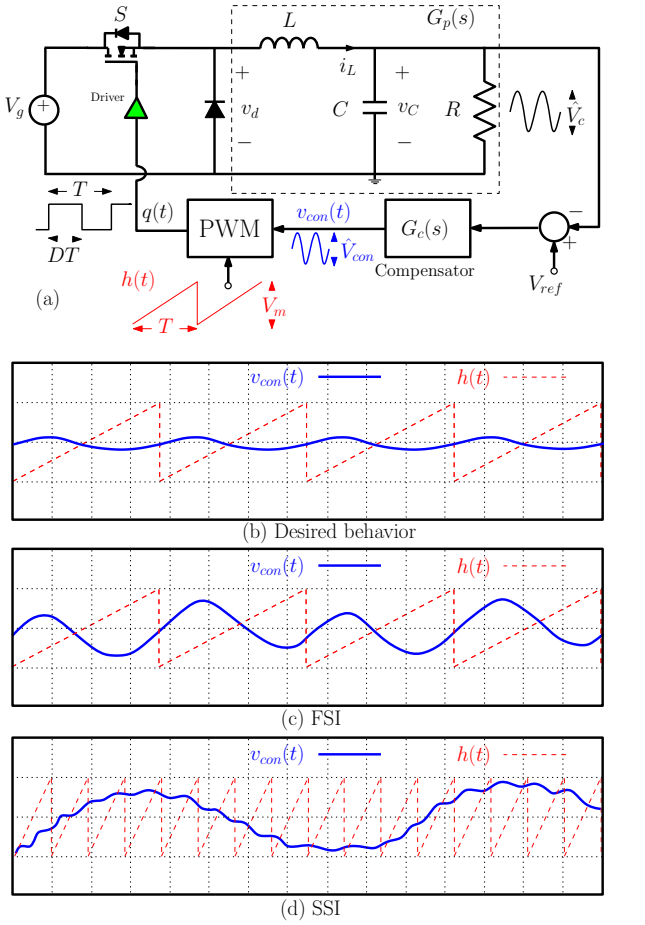

Fig. 1. General circuit diagram of a DC-DC buck converter and the possible instabilities that it can exhibit. (a) the system under voltage-mode control with a compensator with transfer function $G_c(s)$ and a PWM modulator. (b) desired periodic behavior, (c) subharmonic oscillations due to fast scale instability (FSI) and (d) low frequency oscillations due to slow scale instability (SSI) .

This work was received . . . . . ., revised . . . . . .

E. Rodriguez, F.Guinjoan and E. Alarcon are with the Electronic Department of Barcelona Tech (UPC), Barcelona, Spain (e-mail:enricv,guinjoan,ealarcon@eel.upc.edu).

A. El Aroudi is with the Departament d'Enginyeria Electrònica, Elèctrica i Automàtica, of Universitat Rovira i Virgili, Tarragona, Spain (e-mail:abdelali.elaroudi@urv.cat).

This work was partially supported by the Spanish Ministerio de Educación e Innovación under grant TEC-2007-67988-C02-02 and DPI2009-14713-C03-02.

amplitude and low frequency [6], [7]. This phenomenon can effectively be predicted by traditional averaging techniques.

A notable effort has been devoted to modeling these types of behaviors in DC-DC converters. The most well established approach for predicting instabilities in these systems is the average model [8]. However, despite its advantageous design-oriented circuit-based perspective, this model cannot predict all kinds of instabilities, particularly FSI, due to its low-pass averaging nature. Investigations on FSI have been mainly tackled by means of discrete-time recurrent maps [4], [9], [10], capturing accurately the switching nature of the system dynamical behavior. However, such models lack a design-oriented perspective, allowing only a numerical characterization of stability boundary and requiring sophisticated mathematical tools. Regardless of the general applicability of discrete-time models, simplified models for predicting such instabilities in peak current-mode controlled converters have been obtained in order to facilitate their design, in which the occurrence of FSI is common [11]. These simplified models take advantage of the fact that, in current-mode control, the system can be described approximately by a first order model, in such a way that its dynamic response can be derived from simple geometrical techniques, hence developing simple stability conditions to predict FSI [12], and subsequently developing some specific techniques to avoid this undesired behavior such as, for instance, the well-known ramp compensation [13]. This approach can not be applied to voltage-mode control in which the control signal is not of triangular form as in the case of peak current mode control. There is hence still an open challenge regarding the prediction of FSI using a design-oriented standpoint in voltage-mode controlled converters. A harmonic analysis approach has been proposed in [14] in which a closed-form expression for stability is obtained, but this expression cannot be used for design purpose due to its complexity.

On the other hand, the need for analytical tools for predicting such instabilities in voltage-mode controlled converters arises due to new trends in the next-generation power management applications, oriented to further miniaturization and bandwidth extension, which directly implies reducing the ratio between the switching frequency and the natural frequency of the converter, leading the system to be more prone to exhibit FSI and implying that new controllers must be used to obtain a stable system [15], [16].

This work proposes a design-oriented ripple-based index which can capture the effect of all parameters of the converter on the FSI boundary allowing a design-oriented circuit-level standpoint prediction and facilitating further investigation in enhanced controllers oriented to avoid these instabilities [17]. The work is centered in the simple but representative case of a voltage-mode controlled buck converter, however, predicting FSI from design-oriented standpoint can be extended to different topologies and controllers.

The remaining of the paper is organized as follows. Section II presents the ripple-based index hypothesis and validates the approach for the case of a voltage-mode controlled buck converter within a wide range of the design parameter space by means of comparing the boundaries obtained using the ripple index with numerical simulations obtained from the state equations (switched model) and experimental measurements. Section III revisits the stability analysis using discrete-time models and the results obtained from this approach are compared with those obtained from the ripple-based approach hence validating and providing a mathematical support and demonstrating the correctness of the ripple hypothesis. Finally, in Section IV, the approach is validated analytically by using a simplified discrete time model which provides a closed-form design-oriented stability condition which agrees with the initial ripple index hypothesis. Unlike other available results obtained from other existing methods, the stability boundary expression obtained in this work has an analytical form expressed in terms of both the power stage and the controller design parameters. Therefore, one can determine how these parameters are involved in the expressions and, more importantly, how each parameter affects the stability. Finally concluding remarks are drawn in the last section.

II. Ripple-Based Design-Oriented Index: Hypothesis for Predicting Fast-scale Instabilities

With the aim of deriving a design-oriented model to predict FSI, a ripple-based index is proposed for voltage-mode controlled converters, as a complementary tool to average models. This index ρ is defined as the scaled ripple amplitude $\hat{V}_{con}$ of the the control signal $v_{con}(t)$ with respect to the modulator amplitude V_m, therefore compressing the different nature converter design parameters, such as reactive components, control and modulator parameters into a single parameter given by

$$\rho := \frac{\hat{V}_{con}}{V_m} = \frac{\mathcal{F}\hat{V}_C}{V_m} \tag{1}$$

where $\mathcal{F}$ models the effect of the controller upon the ripple amplitude $\hat{V}_C$ of the output capacitor voltage v_C. The ripple index hypothesis is based on the observation that when the ripple instability index (Eq. 1) reaches a critical value ρ_{crit}, FSI is exhibited. Then stability condition is:

$$\rho < \rho_{crit} \tag{2}$$

The next section validates this ripple index hypothesis for the voltage-mode controlled buck converter under a simple PI controller.

A. Validation of the ripple-based approach by means of the switched model

The most widespread configuration, namely a buck converter with PI feedback compensator, shown in Fig. 1, has been chosen to illustrate the validity of the ripple-based approach. Let k_p be the proportional gain of the controller and ω_z its zero. The parameter ω_z has been located at low frequency ($\omega_z < \omega_c$), being $\omega_c = (RC)^{-1}$) in order not to induce SSI. Hence, the effect of the controller upon the converter output voltage ripple is constant ($\mathcal{F} = k_p$) for all frequencies. This choice of the dynamic controller parameters will allow us to be able to analyze independently the effect of the proportional gain k_p and the average value of the control signal on stability.

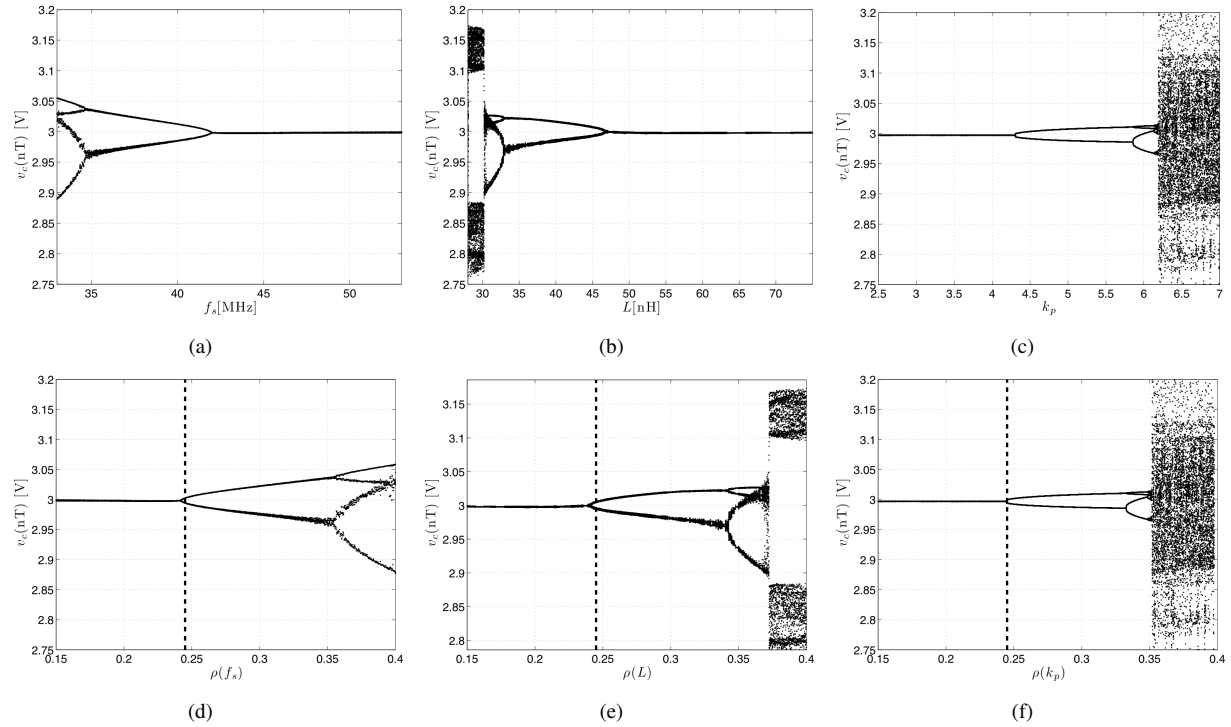

Fig. 2. Bifurcation diagrams obtained by sweeping parameters (a) f_s, (b) L and (c) k_p and its equivalent representation as a function of the ripple-based index ρ (d), (e) and (f), respectively. $\rho_{crit} \approx 0.245$ (dashed line).

Although different expressions for the amplitude of the output voltage ripple may be used, the following simple expression is chosen in order to keep the design-oriented standpoint [1]:

$$\hat{V}_c := \frac{V_g D \bar{D}}{8LCf_s^2} \tag{3}$$

where D is the steady state duty cycle of the PWM driving signal $q(t)$ (See Fig. 1(a)) and $\bar{D} = 1 - D$. Accordingly, ρ given in (1) can be expressed as a function of the set of the design parameters as:

$$\rho(V_g, L, C, k_p, f_s, D, V_m) := \frac{k_p}{V_m} \frac{V_g D \bar{D}}{8LCf_s^2} \tag{4}$$

Fig. 2 shows different bifurcation diagrams, obtained from the exact switched state equations, by considering parameters of different nature as bifurcation parameters. In all cases, an exhibition of FSI and period doubling cascade occurs which ends, eventually, to chaotic behavior. The value of the fixed circuit parameters used for Fig. 2 are $V_g = 6$ V, $V_{ref} = 3$ V, $R = 2.5\ \Omega$, $L = 66$ nH, $C = 20$ nF, $f_s = 50$ MHz, $V_m = 1$ V and $k_p = 3$. These values correspond to a miniaturized converter aiming on-chip integration [18], but the selection is representative -through scaling- of any converter with a low ratio of the switching frequency to the converter cutoff frequency, hence exhibiting moderately large ripples. It can be observed in Fig. 2 that by representing the bifurcation diagrams in terms of the corresponding ripple-based index ρ defined in (4), the bifurcation boundary remains practically constant (dashed line in Fig. 2(d),(e),(f)), independently of the swept parameter. Moreover, it can be noted that the system exhibits FSI (period doubling) for a critical value $\rho_{crit} \approx 0.245$ in all figures. Further validation of the ripple-based index approach is carried out in Fig. 3 for a wide range of the design parameter space. This figure shows the stability boundary obtained from numerical simulations of the circuit state equations contrasted with those obtained from the ripple based index. Although the error increases for low values of load resistance R, the relatively low error obtained for the rest of the design parameter space validates this design-oriented approach for predicting FSI. The approach is only considered for the system working in the CCM, then the design parameter space is limited by the DCM condition. The applicability of the ripple-based approach in DCM has been tackled in [19].

Having explored thoroughly the design parameter space, it has been observed that ρ_{crit} is constant, save a dependence upon the duty cycle D. The evolution of ρ_{crit} in terms of the duty cycle is shown in Fig. 4. Therefore, the stability condition to avoid FSI exhibition, in terms of the system parameters, can finally be expressed as:

$$\rho(V_g, D, L, C, k_p, f_s, V_m) < \rho_{crit}(D) \tag{5}$$

This stability condition given in (5) shows the benefit of the ripple-based approach, which allows compressing most of the design-space parameters into a single ripple-based index ρ, providing a design-oriented tool for predicting the effect of each parameter upon stability.

B. Experimental validation

This section validates the ripple-based FSI prediction approach using an experimental prototype. While the previous section parameter values were oriented to miniaturization, in

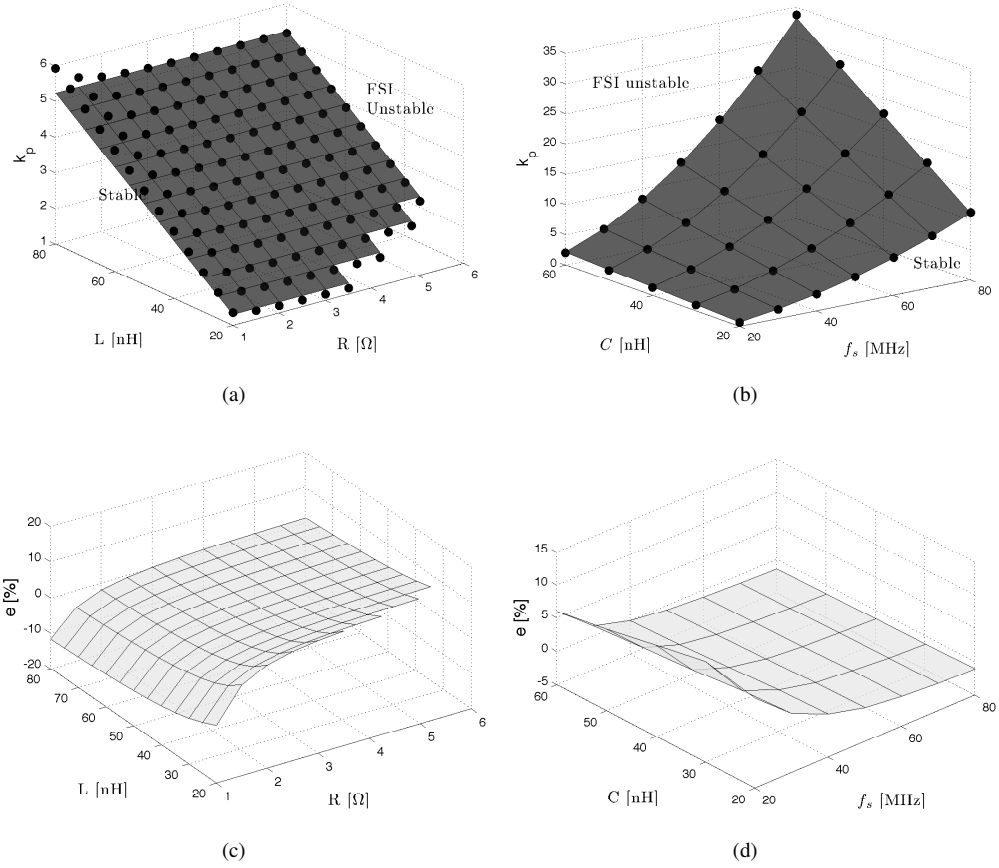

Fig. 3. Stability boundary in the design parameter space obtained from the switched model (black dots) and from the ripple-based index condition (mesh surface) (2) with $\rho_{crit} = 0.245$ by sweeping (a) inductor L, output resistance R and proportional gain k_p and (b) output capacitance C, the switching frequency f_s and proportional gain k_p. The error between the results obtained from the switched model and the ripple-based index condition is shown in (c) and (d), respectively.

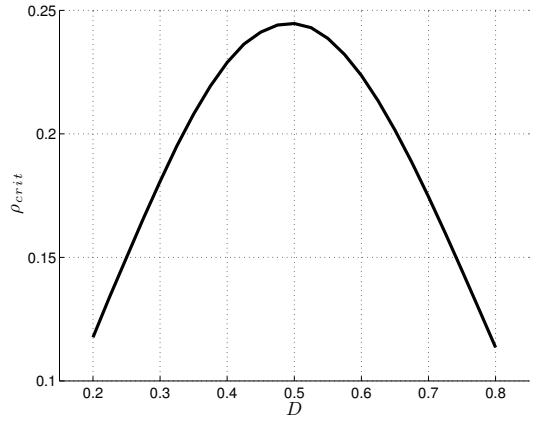

Fig. 4. Evolution of the critical ripple ρ_{crit} leading to FSI in terms of the duty cycle D. The critical value ρ_{crit} is obtained from numerical simulations using the switched model.

this section these values are chosen to facilitate the implementation of the prototype. In Appendix A it is demonstrated that by scaling both the parameters of the reactive elements and the switching frequency, the relative dynamics of the converter remains equivalent [20]. An equivalent set of parameter values used previously and which has been used for the experimental prototype is: $V_g = 6$ V, $R = 2.5\ \Omega$, $L = 33\ \mu$H, $C = 10\ \mu$F, $f_s = 100$ kHz, $V_m = 1.8$ V, $V_{ref} = 3$ V, $k_p = 5.4$.

In Fig. 5 the experimental waveforms of the control voltage signal and the PWM ramp signal just before and just after the exhibition of FSI in the experimental prototype are shown. The dynamics of the system are checked by sweeping the feedback gain k_p and the switching frequency f_s in Fig. 5(a)-(b) and Fig. 5(c)-(d) respectively. In both cases the measured value of the ripple index just at the boundary of stability is found to be $\rho_{crit} \approx 0.27$, which is very close to the critical value of the ripple index obtained from numerical simulations. Regardless of the slight difference between the experimental and the numerical value of ρ_{crit}, which can be attributed to parasitic effects, a deeper exploration of the design parameter space in Fig. 6 shows that the measured critical ripple ρ_{crit} for which FSI occurs remains almost the same within a wide range of the design parameter space.

III. Discrete-time Model Stability Analysis for Predicting FSI and Feedback Ripple Dependence

A. The discrete time model

This section reviews the discrete-time model and its usefulness in predicting FSI boundary in DC-DC converters with the

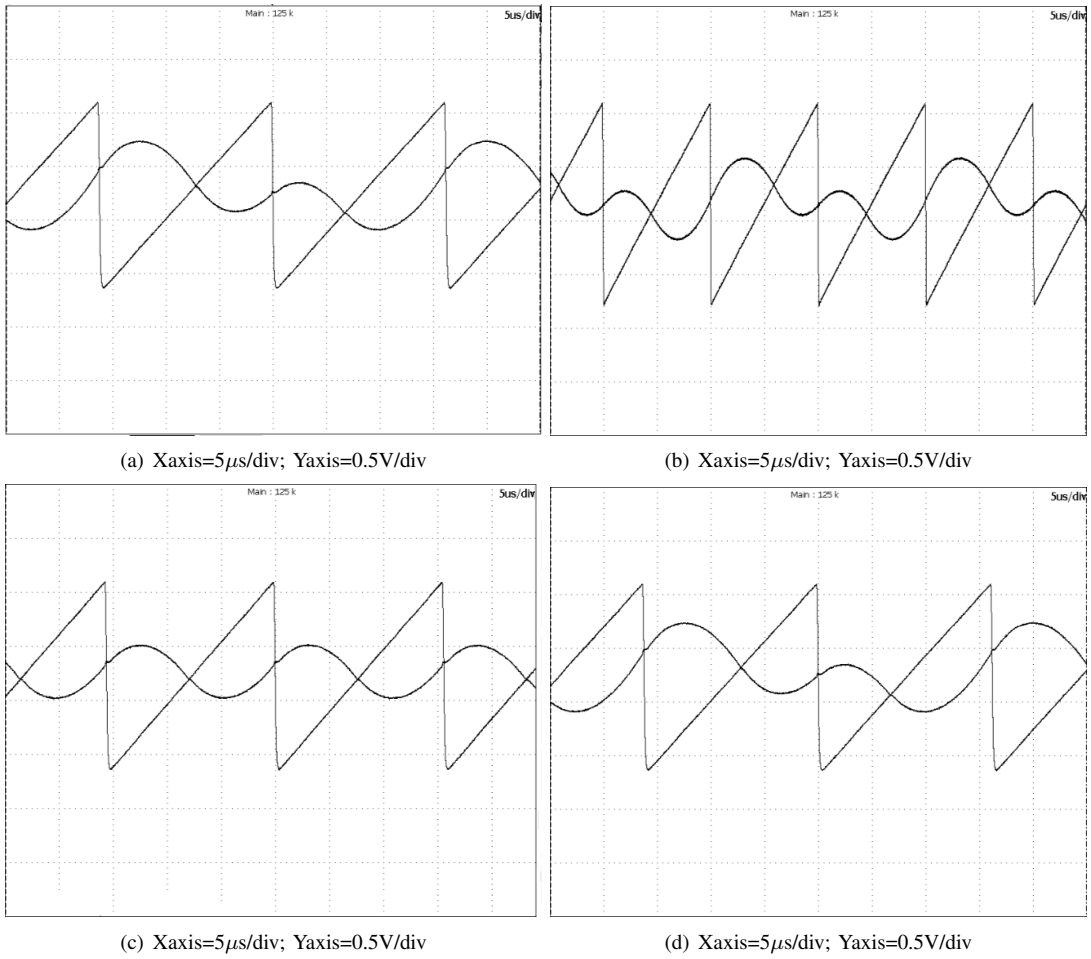

(a) Xaxis=5μs/div; Yaxis=0.5V/div

(b) Xaxis=5μs/div; Yaxis=0.5V/div

(c) Xaxis=5μs/div; Yaxis=0.5V/div

(d) Xaxis=5μs/div; Yaxis=0.5V/div

Fig. 5. Control signal $v_{con}(t)$ and modulator ramp $h(t)$ waveforms just before and just after FSI occurrence by sweeping (a)-(b) k_p and (c)-(d) f_s. Measured critical ripple amplitude at modulator input normalized to ramp amplitude is 0.270 for both cases.

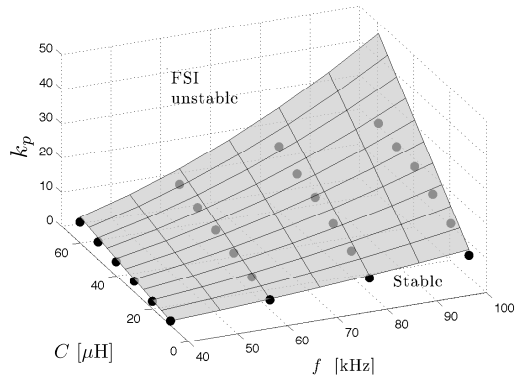

Fig. 6. FSI stability boundary obtained from experimental measurements (black dots) and using ripple index ($\rho_{crit} = 0.245$) (mesh surface) over the design parameter space (k_p, f_s and C).

aim to validate the ripple-based approach by comparing it to the conventional FSI prediction method but also as a starting point for demonstrating its validity, hence giving mathematical support for extending the hypothesis to other topologies. For this purpose, in this section it will be shown that the ripple at the modulator input can be included in the expression of the Jacobian matrix of the discrete-time model of the system. The stability analysis using the discrete-time approach is based on constructing a map, so-called *Poincaré* map, by sampling the dynamics of the converter at each switching period [21]. In order to keep simple expressions, a proportional controller will be used instead of a PI controller in the analysis. In our case, as $\omega_z < (RC)^{-1}$, and as mentioned in [22], an integral term in the controller will not affect the stability boundary of FSI. This is because the zero of the PI controller is placed at low frequencies and in this case the effect of the integral term is just to correct the steady state error while the fast dynamics remains equivalent to that obtained from a proportional controller because one of the eigenvalues remains close to 1. In CCM, the dynamical behavior can be described by the following linear state equations corresponding to each state (ON and OFF) of the switch S driven by the signal $q(t)$ (See Fig. 1)

$$\begin{cases} \dot{\mathbf{x}}(t) = \mathbf{A}_1\mathbf{x}(t) + \mathbf{B}_1 & \text{if } S \text{ is ON } (q(t) = 1) \\ \dot{\mathbf{x}}(t) = \mathbf{A}_2\mathbf{x}(t) + \mathbf{B}_2 & \text{if } S \text{ is OFF } (q(t) = 0) \end{cases} \tag{6}$$

The switch S is in the ON state at the beginning of the switching period and switches to OFF at instants such that

$v_{con}(d_nT) = h(d_nT)$, where d_n is the duty cycle, defined as the fraction of time during which the first configuration (ON) holds. For a linear system with constant state matrix $\mathbf{A}_k$ and input vector $\mathbf{B}_k$ and with initial time t_i and final time t_f, an exact solution can be obtained and it is given by the following expression

$$\mathbf{x}(t_f) = e^{\mathbf{A}_k(t_f - t_i)}\mathbf{x}(t_i) + \int_{t_i}^{t_f} e^{\mathbf{A}_k\theta}\mathbf{B}_k d\theta \tag{7}$$

The map $\mathbf{P}$ that relates consecutive samples, namely the state variables $\mathbf{x}_n$ at the beginning of the cycle to $\mathbf{x}_{n+1}$ at the end of the same cycle can be obtained by stacking up the corresponding solutions during each switching cycle and it can be expressed as [5]:

$$\mathbf{x}_{n+1} = \mathbf{P}(\mathbf{x}_n) = \Phi\mathbf{x}_n + \Psi \tag{8}$$

where matrix Φ and vector Ψ are given by

$$\Phi = \Phi_2(\bar{d}_nT)\Phi_1(d_nT), \Psi = \Phi_2(\bar{d}_nT)\Psi_1(d_nT) + \Psi_2(\bar{d}_nT)$$

being

$$\Phi_k(t_k) = e^{\mathbf{A}_k t_k},\ \Psi_k(t_k) = \int_0^{t_k} e^{\mathbf{A}_k\theta}d\theta\mathbf{B}_k \text{ for } k = 1, 2 \tag{9}$$

and $\bar{d}_n = 1 - d_n$. Additionally, the switching condition, which depends upon the control voltage and the sawtooth modulator $h(t)$, can be expressed as

$$\sigma(d_nT) = \mathbf{K}(\mathbf{X}_{ref} - \Phi_1(d_nT)\mathbf{x}_n) - h(d_nT) \tag{10}$$

where $\mathbf{K} = (k_p,\ k_i)$ is the vector of feedback gains, $\mathbf{X}_{ref} = (V_{ref},\ I_{ref})^t$. Note that $k_i = 0$ and $I_{ref} = 0$ for a voltage-mode proportional control.

B. Stability Analysis Using the Discrete Model

The stability analysis is carried out by studying the local behavior of the model in the vicinity of steady-state $\mathbf{x}^*$, thereby extracting a Jacobian matrix $\mathbf{J}$, whose eigenvalues give the amount of expansion and contraction near this fixed point [5]:

$$\mathbf{J} = \mathbf{J}_{\mathbf{x}} - \mathbf{J}_d\mathbf{J}_{\sigma_d}^{-1}\mathbf{J}_{\sigma_{\mathbf{x}}} \tag{11}$$

The partial derivatives appearing in (11) are given by

$$\mathbf{J}_{\mathbf{x}} = \left.\frac{\partial\mathbf{P}}{\partial\mathbf{x}_n}\right|_{d_n=D} = \Phi_1(DT)\Phi_2(\bar{D}T) \tag{12}$$

which is the product of the two state transition matrices corresponding to each switching interval and which models the effect of a small change of the state variables of the system at the beginning of a switching cycle, on the state variables at the end of the same cycle.

$$\mathbf{J}_d = \left.\frac{\partial\mathbf{P}}{\partial d_n}\right|_{d_n=D,\mathbf{x}_n=\mathbf{x}^*} = \Phi_2\Delta\dot{\mathbf{x}}T \tag{13}$$

which corresponds to the effect of the state transition matrix Φ_2 on the discontinuity of the vector field $\Delta\dot{\mathbf{x}}$, and which models the effect of a small change of the value of the duty cycle on the state variables at the end of the same cycle.

$$\mathbf{J}_{\sigma_d} = \left.\frac{\partial\sigma}{\partial d_n}\right|_{d_n=D,\mathbf{x}_n=\mathbf{x}^*} = (-\mathbf{K}\dot{\mathbf{x}}(DT^-) - m_c)T \tag{14}$$

which corresponds to the difference between the slope $-\mathbf{K}\dot{\mathbf{x}}(DT^-)$ of the control signal $v_{con}(t)$ and $m_c = V_m f_s$, that of the PWM sawtooth signal $h(t)$. This is the small signal model of the original nonlinear switching condition (10).

Finally,

$$\mathbf{J}_{\sigma_{\mathbf{x}}} = \left.\frac{\partial\sigma}{\partial\mathbf{x}_n}\right|_{d_n=D} = -\mathbf{K}\Phi_1(DT) \tag{15}$$

which models how an initial small change in the state variables affects the switching condition (10) from cycle to cycle. In the previous equations it was assumed that in steady state, $\mathbf{x}_n = \mathbf{x}^*$, $d_n = D$, $\bar{D} = 1 - D$. Besides, $\dot{\mathbf{x}}(DT^-) = \mathbf{A}_1\mathbf{x}(DT) + \mathbf{B}_1$, $\dot{\mathbf{x}}(DT^+) = \mathbf{A}_2\mathbf{x}(DT) + \mathbf{B}_2$. For the buck converter under voltage-mode control, $\mathbf{x} = (v_C,\quad i_L)^t$ and the matrices $\mathbf{A}_k$ and vectors $\mathbf{B}_k$ $(k = 1, 2)$ are given by

$$\mathbf{A}_1 = \mathbf{A}_2 = \begin{pmatrix} -\frac{1}{RC} & \frac{1}{C} \\ -\frac{1}{L} & 0 \end{pmatrix}, \mathbf{B}_1 = \begin{pmatrix} 0 \\ \frac{V_g}{L} \end{pmatrix}, \mathbf{B}_2 = \mathbf{0} \tag{16}$$

and $\Delta\dot{\mathbf{x}} = \dot{\mathbf{x}}(DT^-) - \dot{\mathbf{x}}(DT^+)$ can be obtained as follows

$$\Delta\dot{\mathbf{x}} = (\mathbf{A}_1 - \mathbf{A}_2)\mathbf{x}(DT) + (\mathbf{B}_1 - \mathbf{B}_2) = \begin{pmatrix} 0 \\ \frac{V_g}{L} \end{pmatrix} \tag{17}$$

Moreover

$$\mathbf{K}\dot{\mathbf{x}}(DT^-) = \mathbf{K}(\mathbf{A}_1\mathbf{x}(DT^-) + B_1 = k_p\dot{v}_C(DT^-) \tag{18}$$

It can be observed that the final expression of the Jacobian matrix is composed mainly by transition matrices of each configuration but it also includes information about the left and the right time derivative at the switching instant and the slope $m_c = V_m f_s$ of the sawtooth PWM signal $h(t)$.

C. Condition for FSI

The characteristic polynomial equation of the Jacobian matrix $\mathbf{J}$ is given by

$$p(\lambda) := \det(\mathbf{J} - \lambda\mathbf{I}) = 0 \tag{19}$$

In the case of two-dimensional system (19) becomes,

$$p(\lambda) := \lambda^2 - \mathrm{tr}(\mathbf{J})\lambda + \det(\mathbf{J}) = 0 \tag{20}$$

where $\det(\cdot)$ and $\mathrm{tr}(\cdot)$ stand for the trace and the determinant respectively. It is well known that FSI occurs when one of the eigenvalues crosses the unit circle at point (-1,0) in the complex plane [21]. Therefore, the stability boundary can be obtained by making $\lambda = -1$ in (20), hence, obtaining

$$p(-1) = 1 + \det(\mathbf{J}) + \mathrm{tr}(\mathbf{J}) = 0 \tag{21}$$

which implies, by substituting $\mathbf{J}$ by its expression in (11), that

$$\mathbf{J}_{\sigma_d} = \frac{1 + \mathrm{tr}(\Phi) + \det(\Phi)}{\mathbf{K}\Delta\dot{\mathbf{x}}\Phi} \tag{22}$$

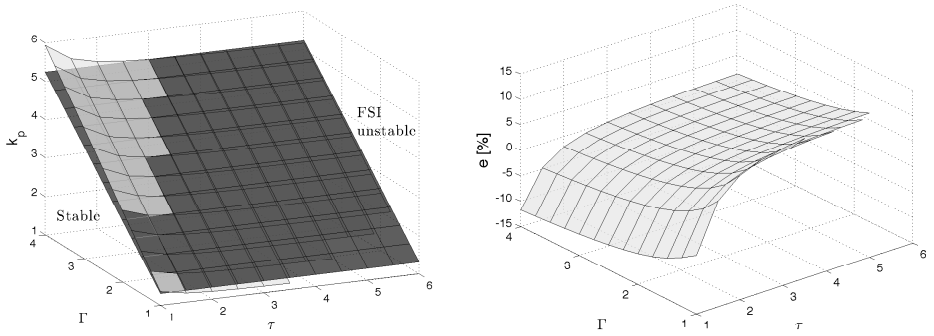

(a) (b)

Fig. 7. (a) FSI boundary surfaces obtained from the discrete-time model (white) and the ripple-based index approach (black) by sweeping the proportional gain k_p, Γ, and τ. (b) Error between both surfaces.

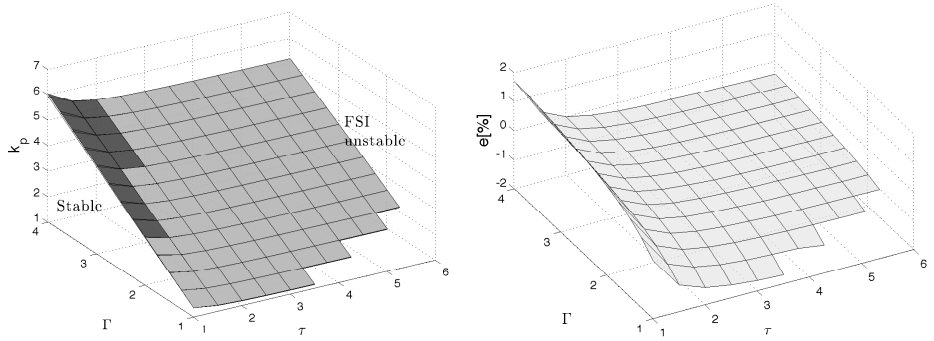

(a) (b)

Fig. 8. FSI boundary surfaces obtained from the exact discrete-time model (black) and by approximating $\dot{v}_C(DT^-)$ (white) the derivative of the output voltage at the switching instant by sweeping feedback gain k_p, Γ and τ. (b) Error between both surfaces.

Solving this equation for a certain design parameter, the FSI boundary corresponding to this parameter can be obtained.

Having presented the nonlinear discrete-time model and its Jacobian matrix for the voltage-mode controlled buck converter, it is possible to compare the results obtained from it with those obtained from the ripple-based index. According to Appendix A, the whole converter design parameter space can be explored by sweeping only two parameters, namely, $\tau = f_s RC = f_s/\omega_c$ and $\Gamma = LCf_s^2$. Fig. 7 shows a comparison between the boundary surfaces obtained from both approaches in such normalized design parameter space. Note that, for low values of τ, the error increases, which is in good concordance with the results previously obtained in Fig. 3 stating that the ripple-based index is not accurate enough for low values of R.

D. Stability analysis including the ripple amplitude

After validating that the ripple-based index approach and the discrete-time model give similar stability boundaries in terms of FSI, this section will establish a relationship between the ripple at the input modulator and the Jacobian matrix of the discrete-time model. In Appendix B, it is demonstrated that this slope and the ripple amplitude are proportional and they are related by the following relationship:

$$\dot{v}_C(DT^-) = 4f_s\hat{V}_C \tag{23}$$

Revisiting the different terms composing the Jacobian matrix (11), it is possible to observe that $\mathbf{J}_{\sigma d}$ contains the derivative of the state variables at the switching instant and therefore, from (23), it also contains the ripple information.

Fig. 8 shows the stability surfaces obtained from the discrete-time model and imposing FSI condition (22), by using the exact value of the derivative at the switching instant and and also by substituting it by the expression in (23), which includes the feedback ripple as its indirect estimate. The error between both surfaces is very small, hence demonstrating the accuracy of the ripple as an estimate of the time derivative at the switching instant. Note that the approximation error starts to increase for low values of τ but depends slightly upon Γ.

IV. Design-Oriented Ripple-Based Index Mathematical Demonstration

A. Revisiting the state transition matrices

The previous section has validated the ripple approach through contrasting the results with the discrete-time model and also unveils that the ripple can be included in the Jacobian

matrix by means of its relation with the PWM switching condition. Nevertheless, it is also apparent that this approach involves sophisticated analysis, that is not of practical engineering use. On the other hand, the ripple-based approach, which has been validated in-depth for the complete design space in section II, is based on a starting hypothesis and lacks a solid mathematical justification. This section will derive the ripple-based FSI index approach from the discrete-time model, taking advantage of the fact that the previous section demonstrates that the ripple of the control signal can be included in the Jacobian matrix of this model. The aim of such demonstration is to give a mathematical support to obtain a closed-form expression for the stability boundary [23] and to examine the accuracy of such approach. The simplification of this matrix is carried out for the particular case of a voltage-mode controlled buck converter with a proportional compensator. In comparison with previous works (for example [24]), which also addressed the issue of obtaining a closed-form expression, the derived expressions are complicated since practical considerations were not used, thus making difficult their interpretation to derive useful design criteria for practical engineering use. In this section such practical considerations will be taken into account in deriving the state transition matrix, corresponding to each linear configuration used by the converter, and therefore in obtaining simplified, but accurate enough, practical expressions for the Jacobian matrix. First, the state transition matrix $\mathbf{\Phi}_k(t)$, which relates the final state $\mathbf{x}(t_f)$ to the initial conditions $\mathbf{x}(t_i)$ during each time interval, is obtained. Using the expression of (7), although very accurate, do not allow to obtain clear design conditions. Instead of using an exact expression of the transition matrix, an approximated expression, by considering practical circuit conditions will be used. Let us first write the solution in its general form as follows

$$\mathbf{x}(t_f) = \mathbf{x}(t_i) + \int_{t_i}^{t_f} (\mathbf{A}_k \mathbf{x}(\theta) + \mathbf{B}_k) d\theta, \quad k = 1, 2 \tag{24}$$

By particularizing for the buck converter of Fig. 1, and considering the ON configuration ($k = 1$), the following expression of the solution can be derived

$$\begin{pmatrix} v_C(t_f) \\ i_L(t_f) \end{pmatrix} = \begin{pmatrix} v_C(t_i) \\ i_L(t_i) \end{pmatrix} + \int_{t_i}^{t} \begin{pmatrix} \dfrac{i_L(\theta)}{C} - \dfrac{v_C(\theta)}{RC} \\ V_g - v_C(\theta) \end{pmatrix} d\theta \tag{25}$$

The simplified transition matrix will be obtained by taking into account the DC-DC buck converter circuit considerations i.e, piecewise linear (triangular) inductor current waveforms and therefore a parabolic shape for the voltage ripple waveforms. Note that the classical pure mathematical exponential matrix simplification based on the Taylor expansion $e^{\mathbf{A}_k t} = \mathbf{I} + \mathbf{A}_k t + (\mathbf{A}_k t)^2 (2!)^{-1} + \ldots$ does not make such a distinction between the two state variables. This circuit-based consideration allows to obtain a considerable simplification, but with high accuracy, by reducing the number of terms into the final expression of the state transition matrices involved in the expression of the Jacobian matrix. In the case of the buck converter, an approximated expression of $\Phi_k(t)$ is given by

$$\tilde{\Phi}_k(t) = \begin{pmatrix} 1 - \dfrac{t}{RC} & \dfrac{t}{C} - \dfrac{t^2}{2RC} \\ -\dfrac{t}{L} & 1 - \dfrac{t^2}{2LC} \end{pmatrix} \tag{26}$$

Also, $\mathbf{A}_1 = \mathbf{A}_2$ which implies $\Phi_1(t) = \Phi_2(t)$ and therefore the matrix $\Phi = \Phi_2(\bar{D}T)\Phi_1(DT)$ in (11) can be approximated by a simpler matrix $\tilde{\Phi}$ given by

$$\tilde{\Phi} = \begin{pmatrix} 1 - \dfrac{T}{RC} & \dfrac{T}{C} - \dfrac{T^2}{2RC} \\ -\dfrac{T}{L} & 1 - \dfrac{T^2}{2LC} \end{pmatrix} \tag{27}$$

Each term involved in the expression of the Jacobian (11) is reviewed according to the previous simplification. Finally, by using the same expression as in (19) along with FSI condition (22), and the aforementioned simplified terms, including the ripple as an estimate of the derivative at the switching instant (23), a closed-form expression for predicting FSI boundary as a function of the ripple amplitude $\hat{V}_C$, is obtained

$$-(4k_p f_s \hat{V}_C + V_m f_s) \frac{4LCf_s}{k_p V_g \mathcal{P}_v} = -1 \tag{28}$$

Let $\omega_0 = (LC)^{-\frac{1}{2}}$. Then, $\mathcal{P}_v$ is given by the following expression

$$\mathcal{P}_v = \frac{2\omega_0^2 \omega_c T^3 D^2 \bar{D}^2 + 4T^2(\omega_c^2 - \omega_0^2) D\bar{D}^2 + 8 - 4T\omega_c}{T^4 \omega_0^4 D^2 \bar{D}^2 - 4T^2(\omega_c^2 - \omega_0^2) D\bar{D} + 8 - 4T\omega_c} \tag{29}$$

B. Critical ripple expression

The closed-form expression (28) still lacks design-oriented standpoint. With the aim of obtaining a simple closed-form expression, the ripple amplitude is approximated as in (3), which has been validated in the whole design parameter space in Appendix C, along with considering $\mathcal{P}_v = 1$. Then, (28) can be rewritten as:

$$\frac{k_p V_g \omega_0^2}{4V_m f_s^2}(1 - 2D\bar{D}) = 1 \tag{30}$$

To make this expression consistent with the ripple-based approach, let us multiply both sides of (30) by $D\bar{D}$ and divide them by $1 - 2D\bar{D}$, obtaining the following final condition for FSI

$$\underbrace{\frac{k_p V_g \omega_0^2 D\bar{D}}{8V_m f_s^2}}_{\rho} = \underbrace{\frac{D\bar{D}}{2 - 4D\bar{D}}}_{\rho_{crit}} \tag{31}$$

The system will be stable if $\rho < \rho_{crit}$. The left side of this equation is the defined ripple-based index ρ while its right side gives the critical ripple value ρ_{crit} for which the system will exhibit FSI. Note that ρ_{crit} depends only on the duty cycle D and its dependence in terms of this parameter is as it is shown previously in Fig. 4 which was obtained from numerical simulations. The stability curve obtained from the exact Jacobian matrix (11) together with those obtained from

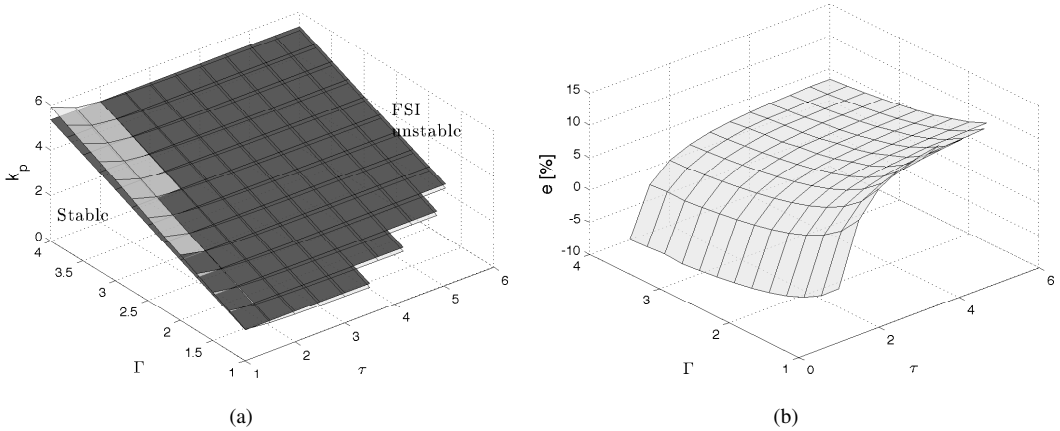

(a) (b)

Fig. 9. FSI boundary surfaces obtained from the discrete-time model ((11), white) and from the ripple-based condition given in (31), black) as a function of gain k_p, τ and Γ. (b) Error between both surfaces.

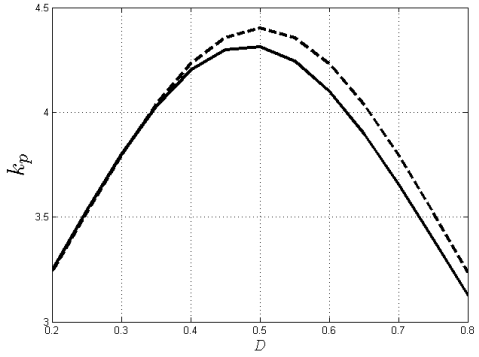

Fig. 10. FSI boundary curves obtained from the discrete-time model ((11), solid) and from the ripple-based condition given in ((31), dashed) with $\mathcal{P}_v = 1$ as a function of the duty cycle D and the proportional gain k_p with τ=2.5 and Γ=3.3.

the ripple index ρ (31) are shown in Fig. 9 by sweeping the parameters k_p, τ and Γ. The results unveils that the error produced by the approximation is negligible in a wide range of the design parameter space. The stability curve obtained from the exact Jacobian matrix (11) and approximated Jacobian (31) with $\mathcal{P} = 1$ by sweeping D and calculating the critical value of the feedback gain k_p is depicted in Fig. 10 showing the accuracy of the closed-form expression for the whole practical range of duty cycle D.

C. Ripple-based index approach limitations

The previous section has given a consistent mathematical demonstration of the ripple-index approach for predicting FSI. However, this approach is not accurate enough in predicting FSI boundary when some design parameters, namely Γ and τ, are relatively low as it is shown in Fig. 9. This is considered to be a penalty to having a simplified expression with the important advantage of being oriented to design. This error due to the different approximations done in the process of obtaining the closed-form expression for predicting FSI yielding to different sources of error. First, the ripple has been included in the discrete-time model as an estimate of the derivative of the state variable at the switching instant. As it can be observed in Appendix B, τ is the parameter that produces a major error (although it is only of 1%). Note that τ is related to the output load of the converter, so that low values of τ ($\tau << 1$) indicates that it is no more valid the assumption, which has been used for relating the output voltage ripple to the derivative of such signal at the switching instant, that the inductor ripple current flows mostly through the output capacitor, hence notably increasing the error when using the ripple-based approach

On the other hand, in order to keep the design-oriented formulation, the ripple has been approximated by (3). In Appendix B (Fig. 15) it has been demonstrated that both parameters have an impact on this approximation, but the error is very low ($< 2\%$). Finally, the last approximation has been done by simplifying the Jacobian matrix using circuit considerations. This is the approximation which introduces more error, since both Γ and τ have an important impact on the approximation of the discrete-time model and when these parameters are low ($\Gamma < 1$ and $\tau < 1$), the error increases as it is shown in Fig. 9 and starting to lose the approach validity.

V. Conclusions

A ripple-based design-oriented approach has been proposed for predicting subharmonic oscillations in switching DC-DC converters under voltage-mode control with fixed frequency PWM modulation strategy. The stability of the system can be ensured by choosing appropriate value of the ramp slope (amplitude and frequency), proportional gain k_p and zero frequency ω_z of the compensator according to the value of the duty cycle D, and resonance frequency ω_0. A simple inspection of the expressions of the critical curves (stability boundaries) reveals that both power stage and controller parameters have to be chosen appropriately to avoid FSI. The system will be stable if the ripple-based index ρ is smaller than the critical ripple ρ_{crit} which only depends on the steady state duty cycle D.

Unlike other available results published in the literature for predicting FSI in a voltage-mode controlled converter, obtained from other existing methods, the stability boundary in this work is expressed in closed-form in terms of all parameters involved in the dynamical model of the system. Moreover, the approach allows to determine how each one of these parameters affects the stability of the system. The approach is validated by numerical simulations from the state equations and also experimentally within a wide range of design parameter space.

The approach used in this work can be extended to other more complex converters. Future works will deal with the application of the proposed approach to this kind of systems as well as its extension to other DC-DC power converters like DC-DC boost and buck-boost converters and other more complex power circuits such as multi-phase and multi-level converters. Work towards designing enhanced controllers that can avoid FSI and SSI by taking advantage of this ripple-centric study is in progress and the results will be reported in a further study.

APPENDICES

A. DYNAMICS EQUIVALENCE OF BUCK SWITCHING CONVERTER

This section demonstrates the equivalence of the dynamical behavior of different buck converters with the same value of dimensionless parameters τ and Γ and with different physical parameters, R, L, C, T, V_g, hence allowing to reduce the number of parameters in the design parameter space. The frequency response of the RLC second order filter can be described as:

$$G_p(s) = \frac{\omega_0^2}{s^2 + \omega_c s + \omega_0^2} \tag{A-1}$$

Therefore, the whole dynamics of the power plant can be characterized by the two parameters ω_0 and ω_c. Note that the buck converter is equivalent to a second order low pass filter with a square wave signal (the diode voltage v_d) at its input which can be described with a particular switching frequency $\omega_s = 2\pi f_s$. Let us define $\tau = f_s/\omega_c = RCf_s$ and $\Gamma = f_s^2/\omega_0^2 = LCf_s^2$. The definition of these new parameters reduces the dimensions of the design parameter space from five to three, namely, Γ, τ and D, instead of the physical parameters L, C, R, f_s and D. Note that Γ relates the switching frequency and the natural frequency of the system and τ is related with the output load of the converter. Two converters will be dynamically equivalent, despite they have different physical parameter values, whenever they have the same values of parameters Γ, τ and D as it is shown in Fig. 11 which is obtained for the set of parameter values used in numerical simulations and those used in the experimental prototype.

B. RELATION BETWEEN THE DERIVATIVE AND THE RIPPLE OF THE CONTROL SIGNAL

In this appendix it will be demonstrated that the ripple amplitude of the control signal is an indirect estimate of its derivative at the switching instant. In a voltage-mode controlled buck converter, the derivative of the feedback state variable (capacitor voltage), according to Fig. 12, is

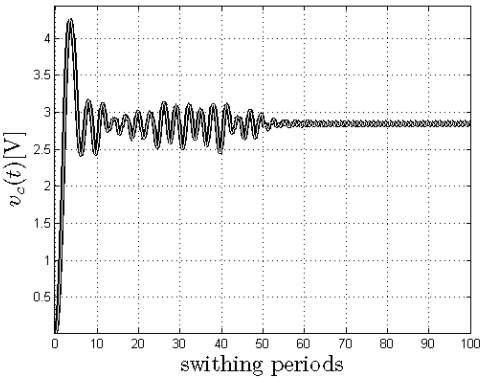

Fig. 11. Transient-simulation of the buck switched model using different values of physical parameters but the same values of dimensionless parameters.

$$\dot{v_c}(DT^-) = \frac{i_C(DT^-)}{C} = \frac{I_{C,max}}{C} \tag{B-1}$$

and its ripple can be expressed as

$$\hat{V}_C = V_{C,max} - V_{C,min} = \frac{1}{C}\int_{t_1}^{t_2} i_C(t)dt = \frac{(t_2 - t_1)I_{C,max}}{2C} \tag{B-2}$$

Note that in the previous equation, it is assumed that the waveform of the capacitor current i_C is triangular. The time duration $t_2 - t_1$ in (B-2) can be obtained by analyzing the following equations

$$\frac{V_g - \bar{V}_C}{L}t_1 = \frac{\bar{V}_C}{L}t_2 \Rightarrow t_2 = \frac{1-D}{D}t_1 \tag{B-3}$$

$$\frac{V_g - \bar{V}_C}{2L}DT = \frac{V_g - \bar{V}_C}{L}t_1 \Rightarrow t_1 = \frac{DT}{2} \tag{B-4}$$

$$t_2 - t_1 = \frac{T}{4} = \frac{1}{4f_s} \tag{B-5}$$

where $\bar{V}_C$ is the average output voltage. Equation (B-3) assumes steady-state while (B-4) assumes zero average capacitor current. Therefore, taking into account the expression of the state-variable derivative in (B-1), (B-2) and (B-5):

$$\dot{v_C}(DT^-) = 4f_s\hat{V}_C \tag{B-6}$$

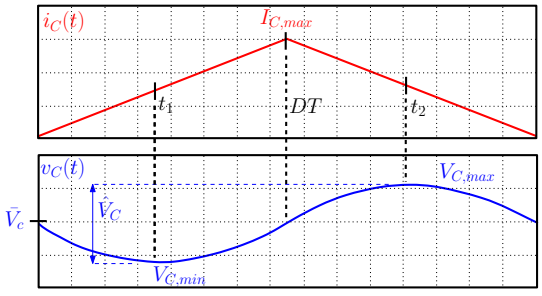

Fig. 12. Ideal representation of the inductor current i_L (top) and output capacitor voltage v_C (bottom) in a buck converter.

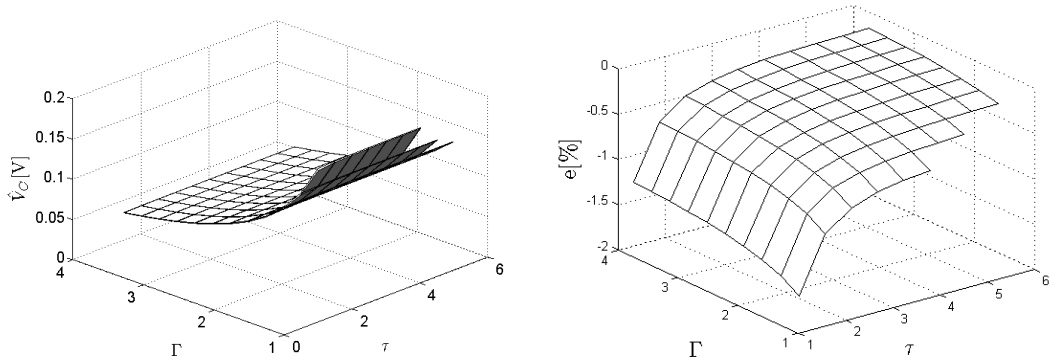

(a) (b)

Fig. 13. Comparison between the ripple amplitude $\hat{V}_C$ in a voltage-mode controlled buck converter by sweeping Γ and τ. (a) From (C-5) (white) and normalized derivative at the switching instant of feedback state variable $\dot{v}_c(DT^-)(4f_s)^{-1}$ (black), (b) error between both results.

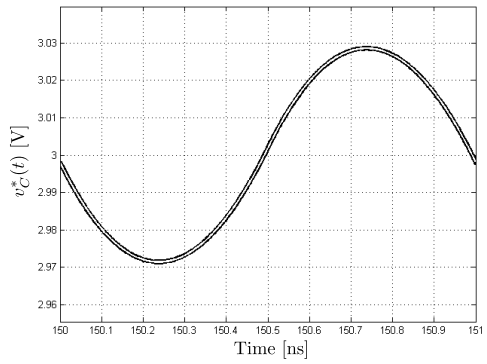

Fig. 14. Theoretical waveforms of the output voltage $v_C^*(t)$ of a buck converter obtained from Eq. (C-5) (with an additional DC voltage V_{ref}) and from simulating the switched model in open-loop.

Fig. 13 validates the approximation by calculating the derivative and the ripple from the exact waveforms, obtained from an exact Laplace analysis of the output ripple, developed in Appendix C, and varying the parameters τ and Γ. Note that the steady state error increases when τ is relatively low, hence losing the validity of the approach.

C. Exact Expression of the Output Voltage Ripple for the Buck Converter from Laplace analysis

A closed-form output voltage ripple expression for the buck converter can be derived using the Laplace transform. The output voltage signal is the result of applying the periodic square wave diode voltage v_d with duty cycle D and amplitude V_g to the RLC second order filter $G_p(s)$, given in (A-1). Therefore, the Laplace transform $V_C(s)$ of the output voltage $v_C(t)$ is given by the product of the transfer function $G_p(s)$ and the Laplace transform $V_d(s)$ of the diode voltage $v_d(t)$

$$V_C(s) = V_d(s)G_p(s) = \frac{(1-e^{-sDT})V_g}{s(1-e^{-sT})}\frac{\omega_0^2}{s^2+\omega_c s+\omega_0^2} \tag{C-1}$$

The partial fraction decomposition of $V_C(s)$ is:

$$V_C(s) = \frac{k_1}{s} + \frac{k_2}{s-a_1} + \frac{k_3}{s-a_2} + \frac{P_0(s)}{1-e^{-sT}} \tag{C-2}$$

where $P_0(s)$ corresponds to the steady-state response and therefore includes the exact output voltage ripple for the buck converter:

$$P_0(s) = (1-e^{-sT})\left(V_C(s) - \frac{k_1}{s} + \frac{k_2}{s-a_1} + \frac{k_3}{s-a_2}\right) \tag{C-3}$$

with $a_1 = -\omega_c/2 - j\omega_d$, $a_2 = -\omega_c/2 + j\omega_d$, $k_1 = DV_g$ and k_2 and k_3 are given by

$$k_2 = V_g\frac{(1-e^{-a_1DT})\omega_0^2}{2a_1(1-e^{-a_1T})j\omega_d}, k_3 = k_2^* \tag{C-4}$$

being $\omega_d = \omega_0\sqrt{1-\xi^2}$. Finally the exact time-domain expression of the steady-state output voltage ripple $v_C^*(t)$ for the buck converter operating in CCM can be written in the following form

$$\begin{aligned} v_C^*(t) \quad &= u(t)V_g\Big[1 - e^{-\omega_c t/2}\left(\cos(\omega_d t) + \tfrac{\xi}{1-\xi^2}\sin(\omega_d t)\right) \\ &\quad -D + \mathcal{K}e^{-\omega_c t/2}\Big[\left(\tfrac{\omega_c}{2}\sin(\omega_d t) + \omega_d\cos(\omega_d t)\right) \\ &\quad -e^{\omega_c T/2}\left(\tfrac{\omega_c}{2}\sin(\omega_d(t+T)) + \omega_d\cos(\omega_d(t+T))\right) \\ &\quad -e^{\omega_c(DT+T)/2}\tfrac{\omega_c}{2}\sin(\omega_d(t+(1-D)T)) + \\ &\quad -e^{\omega_c(DT+T)/2}\omega_d\cos(\omega_d(t+(1-D)T))\Big]\Big] \\ &\quad -u(t-DT)V_g\Big[1 - e^{-\omega_c(t-DT)/2} \\ &\quad \left(\cos(\omega_d(t-DT)) + \tfrac{\xi}{1-\xi^2}\sin(\omega_d(t-DT))\right)\Big] \end{aligned} \tag{C-5}$$

where $\mathcal{K} = (\omega_d - 2\omega_d e^{\omega_c T/2}\cos(\omega_d T) + e^{\omega_c T})^{-1}$. This closed-form expression has been validated by comparing it with the output voltage waveform obtained from numerical simulation of the switched model for an ideal buck converter, as shown in Fig. 14. The waveforms are coincident, thus validating the expression given in (C-5) as an exact description of the converter output ripple for all conditions. From such exact

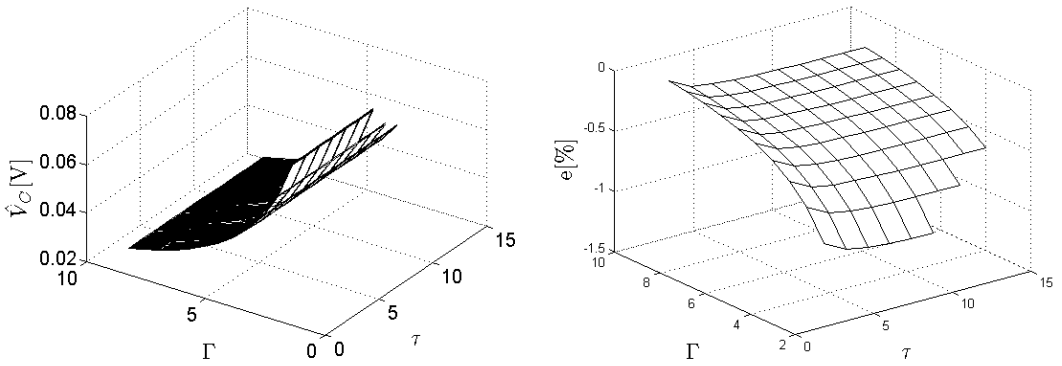

Fig. 15. (a) Voltage ripple amplitude $\hat{V}_C$ from the exact Laplace expression ((C-5), black) and from the approximated expression in Eq. ((3), white) and (b) Error between both results.

ripple expression, it is possible to compare the accuracy of the ripple approximation proposed in (3). The result of this comparison is shown in Fig. 15, in which it is possible to observe that the approximation loses validity for low values of τ and Γ.

REFERENCES

[1] R. W. Erickson and D. Maksimovic, *Fundamentals of Power Electronics*. Lluwer, 2001.

[2] D. C. Hamill and D. J. Jeffries, "Subharmonics and chaos in a controlled switched-mode power converter," *IEEE Transactions on Circuits and Systems*, vol. 35, no. 8, pp. 1059–1061, 1988.

[3] A. El Aroudi and R. Leyva, "Quasi-periodic route to chaos in a PWM voltage controlled DC-DC boost converter," *IEEE Transactions on Circuits and Systems*, vol. 48, pp. 967–987, 2001.

[4] E. Fossas and G. Olivar, "Study of chaos in the buck converter," *IEEE Transactions on Circuits and Systems I: Fundamental Theory and Applications*, vol. 43, no. 1, pp. 13–25, 1996.

[5] A. El Aroudi, M. Debaat, L. Giral, G. Olivar, L. Benadero, and E. Toribio, "Bifurcations in DC-DC swithching converters: reivew of methods and applications," *International Journal of Bifurcation and Chaos (IJBC'05)*, vol. 15, no. 5, pp. 1549–1578, 2005.

[6] A. El Aroudi, L. Benadero, E. Toribio, and G. Olivar, "Hopf bifurcation and chaos from torus breakdown in a PWM voltage-controlled DC-DC boost converter," *IEEE Transactions on Circuits and Systems I: Fundamental Theory and Applications*, vol. 46, no. 11, pp. 1374 –1382, 1999.

[7] S. K. Mazumder, A. H. Nayfeh, and D. Boroyevich, "Theoretical and experimental investigation of the fast- and slow-scale instabilities of a DC-DC converter," *IEEE Transactions on Power Electronics*, vol. 16, no. 2, pp. 201–216, 2001.

[8] R. Middlebrook and S. Cuk, "A general unified approach to modelling switching-converter power stages," in *Power Electronics Specialists Conference (PESC'76)*, 1976, pp. 18–34.

[9] C. Tse, "Flip bifurcation and chaos in three-state boost switching regulators," *IEEE Transactions on Circuits and Systems I: Fundamental Theory and Applications*, vol. 41, no. 1, pp. 16–23, 1994.

[10] G. Papafotiou and N. Margaris, "Calculation and stability investigation of periodic steady states of the voltage controlled buck DC-DC converter," *IEEE Transactions on Power Electronics*, vol. 19, no. 4, pp. 959–970, 2004.

[11] R. Redl and I. Novak, "Instabilities in current-mode controlled switching voltage regulators," in *IEEE Power Electronics Specialists Conference (PESC'81)*, 1981, pp. 17–28.

[12] R. B. Ridley, "A new continuous-time model for current-mode control," *IEEE Transactions on Power Electronics*, p. 382, 1989.

[13] C. Tse and Y. Lai, "Control of bifurcation in current-programmed DC/DC converters: a reexamination of slope compensation," in *IEEE International Symposium on Circuits and Systems (ISCAS'00)*, 2000, pp. 671–674.

[14] C.-C. Fang and E. Abed, "Harmonic balance analysis and control of period doubling bifurcation in buck converters," *IEEE International Symposium on Circuits and Systems (ISCAS'01)*, vol. 2, pp. 209–212, 2001.

[15] G. Villar, E. Alarcon, H. Martinez, D. Biel, E. Vidal, and A. Poveda, "Averaging circuit for switching power converter control: a CMOS current-mode integrated implementation," in *IEEE International Symposium on Circuits and Systems (ISCAS'02)*, 2002, pp. 269 –272.

[16] B. Allard, S. Trochut, X. Lin-Shi, and J.-M. Retif, "Control design for integrated switch-mode power supplies: a new challenge?" in *IEEE Power Electronics Specialists Conference (PESC'04)*, vol. 6, 2004, pp. 4492–4497.

[17] E. Rodriguez, E. Alarcón, H. Iu, and A. El Aroudi, "A frequency domain approach for controlling chaos in switching converters," in *IEEE International Symposium on Circuits and Systems (ISCAS'10)*, 2010, pp. 2928–2931.

[18] G. Villar and E. Alarcon, "Monolithic integration of a 3-level DCM-operated low-floating-capacitor buck converter for DC-DC step-down donversion in standard CMOS," in *IEEE Power Electronics Specialists Conference (PESC'08)*, 2008, pp. 4229–4235.

[19] E. Rodriguez, G. Villar, F. Guinjoan, A. Poveda, A. El-Aroudi, and E. Alarcon, "General-purpose ripple-based fast-scale instability prediction in switching power regulators," in *IEEE International Symposium on Circuits and Systems (ISCAS'07)*, 2007, pp. 2423–2426.

[20] E. Toribio, A. El Aroudi, G. Olivar, and L. Benadero, "Numerical and experimental study of the region of period-one operation of a PWM boost converter," *IEEE Transactions on Power Electronics*, vol. 15, no. 6, pp. 1163–1171, 2000.

[21] M. di Bernardo, F. Garefalo, L. Glielmo, and F. Vasca, "Switchings, bifurcations, and chaos in DC/DC converters," *IEEE Transactions on Circuits and Systems I: Fundamental Theory and Applications*, vol. 45, no. 2, pp. 133–141, 1998.

[22] G. Giaouris, S. Maity, S. Banerjee, V. Pickert, and B. Zahawi, "Application of Filippov method for the analysis of subharmonic instability in DC-DC converters," *Int. J. Circuit Theory Appl.*, vol. 37, pp. 899–919, 2009.

[23] E. Rodriguez, E. Alarcon, and A. El Aroudi, "Demonstration of ripple-based index for predicting fast-scale instability in switching power converters," in *IEEE International Symposium on Circuits and Systems (ISCAS'09)*, 2009, pp. 2653–2656.

[24] M. di Bernardo, F. Garefalo, L. Glielmo, and F. Vasca, "Analysis of chaotic buck, boost and buck-boost converters through switching maps," in *IEEE Power Electronics Specialists Conference, (PESC '97)*, 1997, pp. 754–760.